Journal of Magnetic Resonance 338 (2022) 107189

Contents lists available at ScienceDirect

Journal of Magnetic Resonance

journal homepage: www.elsevier.com/locate/jmr

A B-factor for NOEs?

Peter Güntert

Laboratory of Physical Chemistry, ETH Zürich, 8093 Zürich, Switzerland
Institute of Biophysical Chemistry, Center for Biomolecular Magnetic Resonance, Goethe University Frankfurt, 60438 Frankfurt am Main, Germany
Department of Chemistry, Tokyo Metropolitan University, Hachioji, Tokyo, Japan

ARTICLE INFO

Article history:
Received 7 December 2021
Revised 22 February 2022
Accepted 2 March 2022
Available online 7 March 2022

Keywords:
Distance averaging
Nuclear Overhauser effect
NOE
Internal motion
Thermal motion
B-factor

ABSTRACT

Nuclear Overhauser effects (NOEs) are influenced by motion. Here, we derive exact, analytical results for a model of isotropic, harmonic fluctuations of atom positions that corresponds to the one underlying crystallographic B-factors. The model includes steric repulsion and yields closed-form expressions for the expected value of general invertible functions of the distance between two atoms, with the special case r^{-6} for NOEs. We discuss the implications for the definition of an NOE-based B-factor in solution NMR.

1. Introduction

The nuclear Overhauser effect (NOE) [1–3] plays an outstanding role in NMR spectroscopy, since it provides a way to measure, in a single NOESY experiment [4], a large number of distances in a macromolecule [5], from which its three-dimensional structure can be calculated [6,7]. For two isolated spins in a rigid molecule that undergoes isotropic Brownian motion in solution, the NOE intensity is proportional to r^{-6}, where r is the distance between the two spins [1]. If the molecule is not rigid, averaging occurs as a result of the internal motion. Because of the r^{-6}-dependence of the NOE, this averaging is highly non-linear [8]. NMR spectroscopists are generally aware, in a qualitative sense, of the potentially significant effects of this non-linear averaging, but a quantitative analytical treatment, in analogy to the theory of B-factors (also called atomic displacement parameters or, although somewhat inappropriately [9], temperature factors) in X-ray crystallography [10–12], appears to be lacking, and the question has been addressed mostly through generalized order parameters [8,13] and by numerical methods, e.g. by molecular dynamics simulations [14]. Ambiguous distance restraints in NMR structure calculations [15] make quantitative use of the r^{-6}-dependence of the NOE, but for the different purpose of handling assignment ambiguity and peak overlap in NOESY spectra [16,17]. The recently introduced eNOE approach for an accurate treatment of NOEs in terms of spin diffusion and experimental conditions [18] underlines the importance of an analytical treatment of the effect of thermal fluctuations on the NOE.

Here, we provide analytical formulas for quantification. Although the underlying geometric model of atomic position fluctuations is straightforward, simple approaches, as well as the use of symbolic computation software, were in our hands unsuccessful in providing the desired analytical solutions. We therefore present in this paper explicit derivations and verify their correctness by comparison with numerical simulations. Finally, we discuss the implications of spatial averaging on the NOE and its relationship with crystallographic B-factors.

2. Theory

In this section, we derive exact analytic expressions without and with consideration of steric repulsion for the probability density in Eqs. (8, 21) and the expected value in Eqs. (9–11,22,23) of an invertible function $g(|\vec{x}-\vec{y}|)$ of the distance $|\vec{x}-\vec{y}|$ between two atoms whose positions fluctuate around mean positions, and we evaluate these for the special cases $g(x)=x$ in Eqs. (12, 24), $g(x)=x^2$ in Eqs. (14, 25), $g(x)=x^n$ for any even n in Eq. (15), $g(x)=x^{-6}$ in Eq. (26), and $g(x)=x^{-3}$ in Eq. (27).

2.1. Model

We consider a harmonic oscillator model for the fluctuations of atom positions that is analogous to the one used to derive isotropic B-factors in X-ray crystallography [10–12]. We assume the Carte-

E-mail address: peter.guentert@phys.chem.ethz.ch

https://doi.org/10.1016/j.jmr.2022.107189
1090-7807/

sian coordinates $\vec{x}$ and $\vec{y}$ of the two atoms to be uncorrelated and normally distributed around their respective mean positions $\vec{x}_0$ and $\vec{y}_0$ with standard deviation σ (Fig. 1). The probability density $\rho(\vec{x},\vec{y})$ for finding the first atom at position $\vec{x}$ and the second atom at position $\vec{y}$ is

$$\rho(\vec{x},\vec{y}) = \left(\frac{1}{\sqrt{2\pi}\sigma}\right)^6 e^{-\frac{1}{2}\left(\frac{|\vec{x}-\vec{x}_0|}{\sigma}\right)^2} e^{-\frac{1}{2}\left(\frac{|\vec{y}-\vec{y}_0|}{\sigma}\right)^2} \tag{1}$$

This simple model with independent distributions of the two atoms can be extended to include steric repulsion, i.e. that the atoms cannot come too close to each other. This is essential to treat functions $g(|\vec{x}-\vec{y}|)$ that diverge quickly for vanishing distances $|\vec{x}-\vec{y}| \to 0$, which is the case for NOEs. To take steric repulsion into account, we assume that the atoms must always keep a distance of at least the steric repulsion limit c, and replace the probability density $\rho(\vec{x},\vec{y})$ of Eq. (1) by

$$\rho_c(\vec{x},\vec{y}) = \frac{1}{\kappa_c}\,\rho(\vec{x},\vec{y})\,\Theta(|\vec{x}-\vec{y}|-c), \tag{2}$$

where Θ is the Heaviside function and the normalization constant κ_c is chosen such that $\rho_c(\vec{x},\vec{y})$ is normalized (see Eqs. 18,19 below).

2.2. Probability density of a distance-dependent function

The probability density $\tilde{\rho}(z)$ that a function $g(|\vec{x}-\vec{y}|)$ assumes the value z, is related to the joint probability density $\rho(\vec{x},\vec{y})$ for the atom positions by

$$\tilde{\rho}(z) = \int_{\mathbb{R}^6} \mathrm{d}^3x\,\mathrm{d}^3y\,\rho(\vec{x},\vec{y})\,\delta(g(|\vec{x}-\vec{y}|)-z), \tag{3}$$

where δ denotes the Dirac δ-distribution. To evaluate Eq. (3), we first change variables from $\vec{x}$ and $\vec{y}$ to

$$\vec{u} = \frac{1}{\sqrt{2}}((\vec{x}-\vec{x}_0)+(\vec{y}-\vec{y}_0)), \quad \vec{v} = \frac{1}{\sqrt{2}}((\vec{x}-\vec{x}_0)-(\vec{y}-\vec{y}_0)).$$

which yields for the probability density of Eq. (3),

$$\rho(\vec{x},\vec{y}) = \left(\frac{b}{\pi}\right)^3 e^{-b(\vec{x}-\vec{x}_0)^2} e^{-b(\vec{y}-\vec{y}_0)^2} = \left(\frac{b}{\pi}\right)^3 e^{-b\vec{u}^2} e^{-b\vec{v}^2}, \tag{4}$$

with $b = (2\sigma^2)^{-1}$. The Jacobi determinant of the transformation $T : (\vec{x},\vec{y}) \mapsto (\vec{u},\vec{v})$ is $\det T_* = -1$, where T_* is the matrix of partial derivatives. Let $f(x^2) \equiv g(x)$, $\vec{d} = \vec{x}_0 - \vec{y}_0$, $d = |\vec{d}|$, $v = |\vec{v}|$, and θ be the angle between $\vec{d}$ and $\vec{v}$. Since

$$|\vec{x}-\vec{y}|^2 = |\sqrt{2}\,\vec{v}+\vec{d}|^2 = d^2 + 2v^2 + 2\sqrt{2}\,\vec{d}\cdot\vec{v},$$

we obtain for the probability density of Eq. (3)

$$\begin{aligned}
\tilde{\rho}(z) &= \left(\frac{b}{\pi}\right)^3 \int_{\mathbb{R}^6} \mathrm{d}^3u\,\mathrm{d}^3v\,|\det T_*|\,e^{-b\vec{u}^2}\,e^{-b\vec{v}^2}\,\delta\left(f(|\vec{x}-\vec{y}|^2)-z\right) \\
&= \left(\frac{b}{\pi}\right)^{3/2} \int_{\mathbb{R}^3} \mathrm{d}^3v\,e^{-bv^2}\,\delta\left(f(d^2+2v^2+2\sqrt{2}\vec{d}\cdot\vec{v})-z\right) \\
&= 2\pi\left(\frac{b}{\pi}\right)^{3/2} \int_0^\infty \mathrm{d}v\,v^2 e^{-bv^2} \times \\
&\qquad \int_0^\pi d\theta\,\sin\theta\,\delta\left(f(d^2+2v^2+2\sqrt{2}dv\cos\theta)-z\right) \\
&= 2\pi\left(\frac{b}{\pi}\right)^{3/2} \int_0^\infty \mathrm{d}v\,v^2 e^{-bv^2} \int_{-1}^1 \mathrm{d}x\,\delta\left(f(d^2+2v^2+2\sqrt{2}dvx)-z\right)
\end{aligned} \tag{5}$$

To evaluate the distribution $\delta(f(\alpha+\beta x)-z)$ ($\alpha = d^2+2v^2$, $\beta = 2\sqrt{2}dv$), we use the well-known relation

$$\delta(h(x)) = \sum_{x_k:\,h(x_k)=0} \frac{\delta(x-x_k)}{|h'(x_k)|},$$

where the prime denotes the derivative and the sum runs over all zeros x_k of the function h. Here, $h(x) = f(\alpha+\beta x)-z$. Assuming f to be an invertible function, it follows that the function h has a single zero at $x_1 = (f^{-1}(z)-\alpha)/\beta$, and

$$|h'(x_1)| = \beta|f'(\alpha+\beta x_1)| = \beta\left|f'\left(f^{-1}(z)\right)\right| = \frac{\beta}{\left|(f^{-1})'(z)\right|}.$$

Hence,

$$\delta(f(\alpha+\beta x)-z) = \frac{1}{\beta}\left|(f^{-1})'(z)\right|\,\delta\left(x - \frac{f^{-1}(z)-\alpha}{\beta}\right).$$

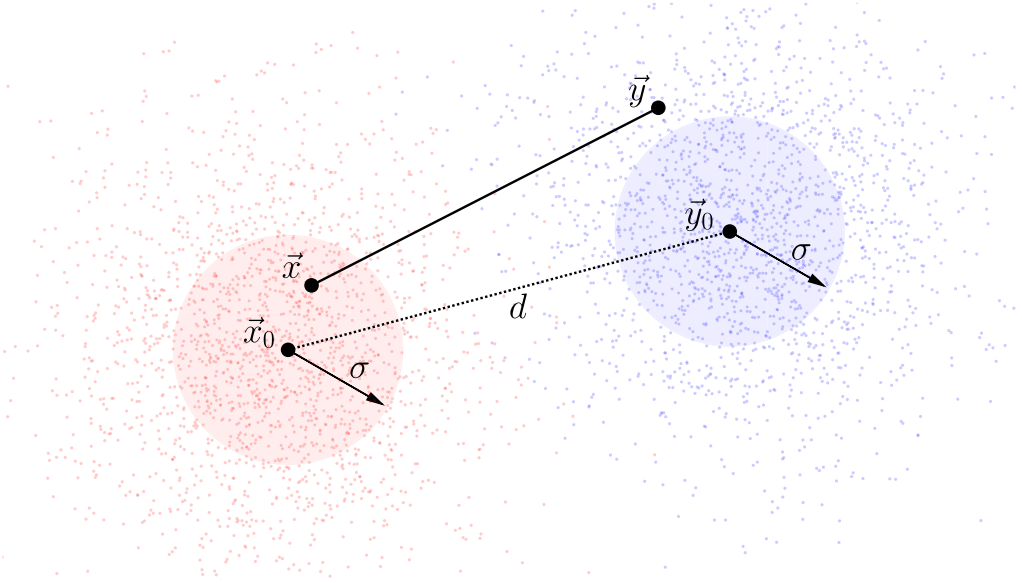

Fig. 1. Illustration of the model for atom fluctuations. We consider functions $g(|\vec{x}-\vec{y}|)$ of the distance $|\vec{x}-\vec{y}|$ between two atoms with position coordinates distributed normally with standard deviation σ around the mean positions $\vec{x}_0$ and $\vec{y}_0$ that are a distance d apart. Colored dots represent 2000 positions sampled from the normal distributions of Eq. (1) with $\sigma = 0.75$ Å and $d = 3$ Å.

Therefore, the second integral in the probability density of Eq. (5) is non-zero if and only if $-1 \leqslant (f^{-1}(z)-\alpha)/\beta \leqslant 1$, which is equivalent to the condition $\beta^2 - (\alpha - f^{-1}(z))^2 \geqslant 0$ and yields

$$\int_{-1}^{1} \mathrm{d}x\, \delta(f(\alpha+\beta x)-z) = \frac{1}{\beta}\left|(f^{-1})'(z)\right| \Theta\left(\beta^2 - (\alpha - f^{-1}(z))^2\right), \qquad (6)$$

Because we have for $w = \sqrt{2}v$

$$\begin{aligned}\beta^2 - (\alpha - f^{-1}(z))^2 &= 4d^2w^2 - (d^2 + w^2 - f^{-1}(z))^2 \\ &= -\left[w^4 + 2(d^2 + f^{-1}(z))w^2 - (d^2 - f^{-1}(z))^2\right] \\ &= -\left[w^2 - \left(d + \sqrt{f^{-1}(z)}\right)^2\right]\left[w^2 - \left(d - \sqrt{f^{-1}(z)}\right)^2\right],\end{aligned}$$

this quantity is positive if the two terms in brackets have opposite signs, and the Heaviside function in Eq. (6) evaluates to

$$\Theta\left(\beta^2 - (\alpha - f^{-1}(z))^2\right) = \begin{cases} 1, & \left|d - \sqrt{f^{-1}(z)}\right| \leqslant w \leqslant \left|d + \sqrt{f^{-1}(z)}\right|; \\ 0, & \text{otherwise.}\end{cases}$$

Using

$$\int_{v_1}^{v_2} \mathrm{d}v\, v e^{-bv^2} = \frac{1}{2}\int_{v_1^2}^{v_2^2} \mathrm{d}x e^{-bx} = \frac{1}{2b}\left(e^{-bv_1^2} - e^{-bv_2^2}\right),$$

we obtain for the probability density $\tilde{\rho}(z)$ of Eq. (5),

$$\tilde{\rho}(z) = \frac{1}{d}\sqrt{\frac{b}{2\pi}}\left|(f^{-1})'(z)\right|\left[e^{-\frac{b}{2}\left(d-\sqrt{f^{-1}(z)}\right)^2} - e^{-\frac{b}{2}\left(d+\sqrt{f^{-1}(z)}\right)^2}\right], \qquad (7)$$

or, switching back from f to g using the relation $f^{-1} = (g^{-1})^2$, the final result

$$\tilde{\rho}(z) = \frac{1}{d}\sqrt{\frac{b}{2\pi}}g^{-1}(z)\left|(g^{-1})'(z)\right|\left[e^{-\frac{b}{2}(d-g^{-1}(z))^2} - e^{-\frac{b}{2}(d+g^{-1}(z))^2}\right]. \qquad (8)$$

Eq. (8) expresses the probability density that the function $g(|\vec{x}-\vec{y}|)$ takes a given value z in closed form.

2.3. Expected value of a distance-dependent function

The expected value of the function $g(|\vec{x}-\vec{y}|)$ is given by

$$\langle g(|\vec{x}-\vec{y}|)\rangle = \int \mathrm{d}z\, \tilde{\rho}(z)\, z,$$

where the integration extends over the values $z = g(|\vec{x}-\vec{y}|)$ taken by the function g. Changing the integration variable to the distance $y = |\vec{x}-\vec{y}| = g^{-1}(z)$, which implies $\mathrm{d}y = |(g^{-1})'(z)|\mathrm{d}z$, and using Eq. (8), one obtains

$$\langle g(|\vec{x}-\vec{y}|)\rangle = \frac{1}{d}\sqrt{\frac{b}{2\pi}}\int_0^\infty \mathrm{d}y\, y\left[e^{-\frac{b}{2}(d-y)^2} - e^{-\frac{b}{2}(d+y)^2}\right] g(y) \qquad (9)$$

$$= \frac{1}{d}\sqrt{\frac{b}{2\pi}}\left\{\int_{-d}^{\infty} \mathrm{d}x\,(x+d)\, g(x+d)\, e^{-\frac{b}{2}x^2} - \int_d^\infty \mathrm{d}x\,(x-d)\, g(x-d)\, e^{-\frac{b}{2}x^2}\right\} \qquad (10)$$

$$= \frac{1}{d}\sqrt{\frac{b}{2\pi}}\int_{-\infty}^{\infty} \mathrm{d}x\,(x+d)\, g(|x+d|)\, e^{-\frac{b}{2}x^2}. \qquad (11)$$

Since $y\left[e^{-\frac{b}{2}(d-y)^2} - e^{-\frac{b}{2}(d+y)^2}\right] = O(y^2)$ asymptotically for $y \to 0$, this expected value exists only if $g(y) = o(y^{-3})$ for $y \to 0^+$.

The expected value of the distance between the two atoms can be calculated as a special case of Eq. (10):

$$\begin{aligned}\langle|\vec{x}-\vec{y}|\rangle &= \frac{1}{d}\sqrt{\frac{b}{2\pi}}\left\{\int_{-d}^{\infty} \mathrm{d}x\,(x+d)^2 e^{-\frac{b}{2}x^2} - \int_d^\infty \mathrm{d}x\,(x-d)^2 e^{-\frac{b}{2}x^2}\right\} \\ &= \frac{d}{\sqrt{\pi}\eta^2}\left\{\int_{-\eta}^{\infty} \mathrm{d}z\,(z+\eta)^2 e^{-z^2} - \int_\eta^\infty \mathrm{d}z\,(z-\eta)^2 e^{-z^2}\right\} \\ &= \frac{d}{\sqrt{\pi}\eta^2}\left\{\int_{-\eta}^{\eta} \mathrm{d}z\,(z^2+\eta^2) e^{-z^2} + 4\eta\int_\eta^\infty \mathrm{d}z z e^{-z^2}\right\} \\ &= d\left\{\left(1+\frac{1}{2\eta^2}\right)\Phi(\eta) + \frac{e^{-\eta^2}}{\sqrt{\pi}\eta}\right\},\end{aligned} \qquad (12)$$

where

$$\eta = d\sqrt{\frac{b}{2}} = \frac{d}{2\sigma}, \qquad \text{and} \qquad \Phi(x) \equiv \frac{2}{\sqrt{\pi}}\int_0^x \mathrm{d}z e^{-z^2} \qquad (13)$$

is the error function. If the spread in the positions of the two atoms goes to zero, i.e. if $\sigma \to 0$ or $\eta \to \infty$, the expected value of the distance between the two atoms becomes equal to d, as expected. For $\sigma > 0$, the average distance is always larger than the distance between the mean atom positions, i.e. $\langle|\vec{x}-\vec{y}|\rangle > d$.

The expected value of the squared distance can be calculated using Eq. (11):

$$\begin{aligned}\langle|\vec{x}-\vec{y}|^2\rangle &= \frac{1}{d}\sqrt{\frac{b}{2\pi}}\int_{-\infty}^{\infty} \mathrm{d}x\,(x+d)^3 e^{-\frac{b}{2}x^2} \\ &= \frac{1}{d}\sqrt{\frac{b}{2\pi}}\int_{-\infty}^{\infty} \mathrm{d}x\,(x^3 + 3dx^2 + 3d^2x + d^3) e^{-\frac{b}{2}x^2} \\ &= \sqrt{\frac{b}{2\pi}}\int_{-\infty}^{\infty} \mathrm{d}x\,(d^2 + 3x^2) e^{-\frac{b}{2}x^2} \\ &= d^2 + \frac{3}{b} = d^2 + 6\sigma^2 = d^2\left(1 + \frac{3}{2\eta^2}\right).\end{aligned} \qquad (14)$$

This result can be verified by the simple reasoning

$$\begin{aligned}\langle|\vec{x}-\vec{y}|^2\rangle &= \langle|(\vec{x}_0-\vec{y}_0) + (\vec{x}-\vec{x}_0) - (\vec{y}-\vec{y}_0)|^2\rangle \\ &= d^2 + \langle|\vec{x}-\vec{x}_0|^2\rangle + \langle|\vec{y}-\vec{y}_0|^2\rangle \\ &= d^2 + 6\langle(x^{(1)} - x_0^{(1)})^2\rangle = d^2 + 6\sigma^2,\end{aligned}$$

which is possible because the distributions of the individual coordinates are assumed to be independent. It follows again that $\langle|\vec{x}-\vec{y}|^2\rangle \to d^2$ ($\eta \to \infty$) and $\langle|\vec{x}-\vec{y}|^2\rangle > d^2$, if $\eta < \infty$.

In general, we obtain from Eq. (11) for $n = 0, 1, \ldots$

$$\begin{aligned}\langle|\vec{x}-\vec{y}|^{2n}\rangle &= \frac{1}{d}\sqrt{\frac{b}{2\pi}}\int_{-\infty}^{\infty} \mathrm{d}x\,(x+d)^{2n+1} e^{-\frac{b}{2}x^2} \\ &= \frac{d^{2n}}{\sqrt{\pi}}\int_{-\infty}^{\infty} \mathrm{d}z\left(1+\frac{z}{\eta}\right)^{2n+1} e^{-z^2} \\ &= \frac{d^{2n}}{\sqrt{\pi}}\sum_{k=0}^{2n+1}\binom{2n+1}{k}\frac{1}{\eta^k}\int_{-\infty}^{\infty} \mathrm{d}z z^k e^{-z^2} \\ &= \frac{d^{2n}}{\sqrt{\pi}}\sum_{k=0}^{n}\binom{2n+1}{2k}\frac{1}{\eta^{2k}}\int_{-\infty}^{\infty} \mathrm{d}z z^{2k} e^{-z^2} \\ &= \frac{d^{2n}}{\sqrt{\pi}}\sum_{k=0}^{n}\binom{2n+1}{2k}\frac{1}{\eta^{2k}}\Gamma\left(k+\frac{1}{2}\right)\end{aligned}$$

Using Legendre's duplication formula (see [19], p. 200)

$$\sqrt{\pi}\,\Gamma(2z) = 2^{2z-1}\,\Gamma(z)\,\Gamma\left(z+\frac{1}{2}\right)$$

we obtain

$$\frac{\Gamma(k+\frac{1}{2})}{(2k)!} = \frac{\Gamma(k+\frac{1}{2})}{\Gamma(2(k+\frac{1}{2}))} = \frac{\sqrt{\pi}}{2^{2k}\,\Gamma(k+1)} = \frac{\sqrt{\pi}}{2^{2k}\,k!}$$

and finally

$$\begin{aligned}\langle|\vec{x}-\vec{y}|^{2n}\rangle &= d^{2n}\left[1+\sum_{k=1}^{n}\frac{(2n+1)!}{k!\,(2n+1-2k)!}\frac{1}{(2\eta)^{2k}}\right]\\ &= d^{2n}\left[1+\sum_{k=1}^{n}\frac{(2n+1)!}{k!\,(2n+1-2k)!}\left(\frac{\sigma}{d}\right)^{2k}\right].\end{aligned} \tag{15}$$

For instance, the expected value of the sixth power of the distance is

$$\langle|\vec{x}-\vec{y}|^{6}\rangle = d^{6}\left[1+42\left(\frac{\sigma}{d}\right)^{2}+420\left(\frac{\sigma}{d}\right)^{4}+840\left(\frac{\sigma}{d}\right)^{6}\right]. \tag{16}$$

2.4. Model including steric repulsion

To study the effect of motional averaging on nuclear Overhauser effects, it is relevant to look at the case $g(x) = x^{-6}$. However, with the uncorrelated normal distributions of the atomic coordinates that have been assumed so far, the expected value diverges, $\langle|\vec{x}-\vec{y}|^{-6}\rangle = \infty$. To obtain a meaningful result, it must be considered that the atoms cannot come too close to each other. To take this into account, we assume that the atoms must always keep a distance of at least c, and replace the probability density $\rho(\vec{x},\vec{y})$ by

$$\rho_c(\vec{x},\vec{y}) = \frac{1}{\kappa_c}\,\rho(\vec{x},\vec{y})\,\Theta(|\vec{x}-\vec{y}|-c) \tag{17}$$

with $0 < c < d$ and κ_c such that $\rho_c(\vec{x},\vec{y})$ is normalized, i.e.

$$\kappa_c = \int_{\mathbb{R}^6} \mathrm{d}^3x\,\mathrm{d}^3y\,\rho(\vec{x},\vec{y})\,\Theta(|\vec{x}-\vec{y}|-c). \tag{18}$$

Taking the derivative with respect to c yields

$$\begin{aligned}-\frac{\mathrm{d}\kappa_c}{\mathrm{d}c} &= \int_{\mathbb{R}^6} \mathrm{d}^3x\,\mathrm{d}^3y\,\rho(\vec{x},\vec{y})\,\delta(|\vec{x}-\vec{y}|-c)\\ &= \frac{1}{d}\sqrt{\frac{b}{2\pi}}c\left[e^{-\frac{b}{2}(d-c)^2}-e^{-\frac{b}{2}(d+c)^2}\right],\end{aligned}$$

or

$$\kappa_c = 1-\frac{1}{d}\sqrt{\frac{b}{2\pi}}\int_0^c \mathrm{d}x\,x\left[e^{-\frac{b}{2}(d-x)^2}-e^{-\frac{b}{2}(d+x)^2}\right].$$

The integral can be evaluated as

$$\begin{aligned}&\int_0^c \mathrm{d}x\,x\left[e^{-\frac{b}{2}(d-x)^2}-e^{-\frac{b}{2}(d+x)^2}\right] =\\ &= \int_d^{d-c}\mathrm{d}y\,(y-d)\,e^{-\frac{b}{2}y^2} - \int_d^{d+c}\mathrm{d}y\,(y-d)\,e^{-\frac{b}{2}y^2}\\ &= \int_{d-c}^{d+c}\mathrm{d}y\,(d-y)\,e^{-\frac{b}{2}y^2}\\ &= d\sqrt{\frac{b}{2\pi}}\left[\Phi\left(\sqrt{b/2}(d+c)\right)-\Phi\left(\sqrt{b/2}(d-c)\right)\right]\\ &\qquad -\frac{1}{b}\left[e^{-\frac{b}{2}(d-c)^2}-e^{-\frac{b}{2}(d+c)^2}\right].\end{aligned}$$

For κ_c one obtains finally

$$\kappa_c = 1-\frac{1}{2}\left[\Phi(\eta_c^+)-\Phi(\eta_c^-)-\frac{1}{\sqrt{\pi}\eta}\left(e^{-\eta_c^{-2}}-e^{-\eta_c^{+2}}\right)\right] \tag{19}$$

with dimensionless

$$\eta = d\sqrt{\frac{b}{2}} = \frac{d}{2\sigma} \qquad \text{and} \qquad \eta_c^{\pm} = \eta\left(1\pm\frac{c}{d}\right). \tag{20}$$

Instead of $\tilde{\rho}(z)$, we obtain the probability density

$$\begin{aligned}\tilde{\rho}_c(z) &= \int \mathrm{d}^3x\,\mathrm{d}^3y\,\rho_c(\vec{x},\vec{y})\,\delta(g(|\vec{x}-\vec{y}|)-z)\\ &= \frac{1}{\kappa_c}\,\tilde{\rho}(z)\,\Theta(\mathrm{sgn}(g')(z-g(c))),\end{aligned} \tag{21}$$

where $\mathrm{sgn}(g')$ denotes the sign of g'. Since we assume the function g to be invertible, $\mathrm{sgn}(g'(x))$ does not depend on x.

2.5. Expected value of a distance-dependent function with steric repulsion

The expected value of the function $g(|\vec{x}-\vec{y}|)$ becomes

$$\begin{aligned}\langle g(|\vec{x}-\vec{y}|)\rangle_c &= \int \mathrm{d}z\,\tilde{\rho}_c(z)\,z\\ &= \frac{1}{\kappa_c d}\sqrt{\frac{b}{2\pi}}\int_c^{\infty}\mathrm{d}y\,y\left[e^{-\frac{b}{2}(d-y)^2}-e^{-\frac{b}{2}(d+y)^2}\right]g(y)\\ &= \frac{1}{\kappa_c d}\sqrt{\frac{b}{2\pi}}\left\{\int_{-d+c}^{\infty}\mathrm{d}x\,(x+d)\,g(x+d)\,e^{-\frac{b}{2}x^2}\right.\\ &\qquad \left.-\int_{d+c}^{\infty}\mathrm{d}x\,(x-d)\,g(x-d)\,e^{-\frac{b}{2}x^2}\right\}\end{aligned} \tag{22}$$

or

$$\begin{aligned}\langle g(|\vec{x}-\vec{y}|)\rangle_c &= \frac{\eta}{\kappa_c\sqrt{\pi}}\int_{c/d}^{\infty}\mathrm{d}x\,x\left[e^{-\eta^2(1-x)^2}-e^{-\eta^2(1+x)^2}\right]g(xd)\\ &= \frac{2\eta e^{-\eta^2}}{\kappa_c\sqrt{\pi}}\int_{c/d}^{\infty}\mathrm{d}x\,x\,e^{-\eta^2x^2}\sinh(2\eta^2x)\,g(xd)\end{aligned} \tag{23}$$

For instance,

$$\langle|\vec{x}-\vec{y}|\rangle_c = \frac{d}{\kappa_c}\left\{\left(1+\frac{1}{2\eta^2}\right)\frac{\Phi(\eta_c^+)+\Phi(\eta_c^-)}{2}+\frac{\eta_c^-\,e^{-\eta_c^{+2}}+\eta_c^+\,e^{-\eta_c^{-2}}}{2\sqrt{\pi}\eta^2}\right\} \tag{24}$$

and

$$\begin{aligned}\langle|\vec{x}-\vec{y}|^2\rangle_c &= \frac{d^2}{\kappa_c}\left\{\left(1+\frac{3}{2\eta^2}\right)\left(1-\frac{\Phi(\eta_c^+)-\Phi(\eta_c^-)}{2}\right)\right.\\ &\quad +\frac{1}{2\sqrt{\pi}\eta^3}\left((1+\eta_c^{-2}+3\eta^2-3\eta\eta_c^-)\,e^{-\eta_c^{-2}}\right.\\ &\quad \left.\left.-(1+\eta_c^{+2}+3\eta^2-3\eta\eta_c^+)\,e^{-\eta_c^{+2}}\right)\right\}.\end{aligned} \tag{25}$$

In the case $g(x) = x^{-6}$ that is relevant for the NOE, one obtains

$$\begin{aligned}\left\langle\frac{1}{|\vec{x}-\vec{y}|^6}\right\rangle_c &= \frac{1}{d^6}\frac{\eta}{\kappa_c\sqrt{\pi}}\int_{c/d}^{\infty}\mathrm{d}x\frac{e^{-\eta^2(1-x)^2}-e^{-\eta^2(1+x)^2}}{x^5}\\ &= \frac{1}{d^6}\frac{2\eta e^{-\eta^2}}{\kappa_c\sqrt{\pi}}\int_{c/d}^{\infty}\mathrm{d}x\frac{e^{-\eta^2x^2}\sinh(2\eta^2x)}{x^5}.\end{aligned} \tag{26}$$

Eq. (26) describes the averaging of the NOE in closed form. No approximations were made in deriving Eq. (26) and all preceding results. These are therefore exact for the given model. The integral in Eq. (26) cannot be expressed by elementary functions; it has to be evaluated by numerical integration.

The analogous result for $g(x) = x^{-3}$, which bears relevance for the averaging of the NOE in the fast motion regime [20], is

$$\begin{aligned}\left\langle\frac{1}{|\vec{x}-\vec{y}|^3}\right\rangle_c &= \frac{1}{d^3}\frac{\eta}{\kappa_c\sqrt{\pi}}\int_{c/d}^{\infty}\mathrm{d}x\frac{e^{-\eta^2(1-x)^2}-e^{-\eta^2(1+x)^2}}{x^2}\\ &= \frac{1}{d^3}\frac{2\eta e^{-\eta^2}}{\kappa_c\sqrt{\pi}}\int_{c/d}^{\infty}\mathrm{d}x\frac{e^{-\eta^2x^2}\sinh(2\eta^2x)}{x^2}.\end{aligned} \tag{27}$$

2.6. Numerical simulation

The analytical results obtained so far can be corroborated by numerical simulation. To this end, we generate a large number n of samples of positions $\vec{x}^{(i)}$ and $\vec{y}^{(i)}$ $(i = 1,\ldots,n)$ from normal distributions with standard deviation σ, centered, without loss of generality, at $\vec{x}_0 = (0,0,0)$ and $\vec{y}_0 = (d,0,0)$, and subject to the the

condition $|\vec{x}^{(i)} - \vec{y}^{(i)}| > c$. We can then approximate the expected value of the function $g(|\vec{x} - \vec{y}|)$ by

$$\langle g(|\vec{x} - \vec{y}|)\rangle_c \approx \frac{1}{n}\sum_{i=1}^{n} g(|\vec{x}^{(i)} - \vec{y}^{(i)}|) \tag{28}$$

3. Results

Results can be given in universal manner by scaling all parameters by the distance d between the centers of the normal distributions of the two atom positions, i.e., by assuming units for which $d = 1$.

The influence of steric repulsion on the distribution of atom positions is in most cases small, as evidenced by values of the normalization constant κ_c close to one (Table 1). The normalization constant κ_c is a measure of the accessible configuration space, relative to the configuration space that the two atoms could occupy without steric repulsion. In all cases, $\kappa_c < 1$ because steric repulsion decreases the accessible configuration space. The smallest value $\kappa_c = 1/2$ is obtained for $c = d$ in the limit $\sigma \to 0$, where exactly half the original configuration space becomes inaccessible.

The average value $\langle|\vec{x} - \vec{y}|\rangle_c$ of the distance between two atoms with thermal fluctuations that can be modeled by normal distributions is obtained from Eq. (12) if the fluctuations of the two atom positions are totally independent from each other, or from Eq. (24) if steric repulsion is considered. Numeric values are given in Table 2 and plotted in Fig. 2a. They show, as expected, that $\langle|\vec{x} - \vec{y}|\rangle_c$ is close to d for small amplitude fluctuations. For medium fluctuation sizes, e.g., $\sigma = 0.5d$, the average values increase significantly because there are more configurations with $|\vec{x} - \vec{y}| > d$ than $|\vec{x} - \vec{y}| < d$. For (unrealistically) large standard deviations $\sigma \gg d$, the average distance becomes proportional to σ, i.e., $\langle|\vec{x} - \vec{y}|\rangle_c \approx 4\sigma/\sqrt{\pi} \approx 2.26\sigma$. The effect of steric repulsion is minimal, the average distance values in Table 2 increase only very little with increasing steric repulsion limit c.

The picture is similar for the root-mean-square distance $\langle|\vec{x} - \vec{y}|^2\rangle_c^{1/2}$ that is given for selected values of the standard deviation σ and the steric repulsion limit c in Table 3, and plotted in Fig. 2b.

In the case $\langle|\vec{x} - \vec{y}|^{-6}\rangle_c$ that is relevant for NOEs and shown in Table 4 and plotted in Fig. 3a, the situation is quite different. Because of the r^{-6}-dependence, it is the small distance values that dominate the calculation of the expected value. Hence, the steric repulsion limit becomes an important parameter with a practically relevant value of $c \approx 2$ Å, given by twice the repulsive core radius of a hydrogen atom. In fact, $\langle|\vec{x} - \vec{y}|^{-6}\rangle_c$ diverges if steric repulsion is not taken into account. The effect of averaging can be very pronounced, as can be seen, for instance, for $d = 5$ Å, $\sigma = 1$ Å, and $c = 2$ Å (corresponding to $\sigma = 0.2d$ and $c = 0.4d$ in Table 4), where the NOE is expected to be about 3.6 times stronger than in the absence of internal motion. On the other hand, $\langle|\vec{x} - \vec{y}|^{-6}\rangle_c$ becomes very small for large values of the standard deviation σ, i.e., NOEs are quenched by large atom position fluctuations as they occur, for instance, in flexible tails and disordered loops in proteins, where typically only very short-range NOEs can be observed.

When NOEs are used to obtain distance restraints for NMR structure calculations, they are traditionally converted into upper distance bounds according to a r^{-6} relationship using the isolated spin pair approximation. In the presence of internal motion, this can lead to incorrect distances. The effect can be quantified by the "effective" distance

$$d_{\text{eff}} = \langle|\vec{x} - \vec{y}|^{-6}\rangle_c^{-1/6}. \tag{29}$$

Values of d_{eff} are given for selected values of the standard deviation σ and the steric repulsion limit c in Table 5, and plotted in Fig. 3b. Specific examples are given in Fig. 4 for a strong, medium, and weak NOE ($d = 2.4$, 3.5, and 5.0 Å, respectively), fixed $c = 2$ Å, and σ in the range of 0–8 Å.

For small σ, d_{eff} is close to the distance d between the mean positions, whereas intermediate values of σ may lead to an underestimation of the true distance between the centers of the atom distributions, for instance by 20% for $d = 5$ Å, $\sigma = 1$ Å, and $c = 2$ Å (corresponding to $\sigma = 0.2d$ and $c = 0.4d$ in Table 5). For even larger σ, the effective distance significantly overestimates

Table 1
Values of the normalization constant κ_c of Eq. (19) for different standard deviations σ and steric repulsion limits c.

σ/d	$c = 0$	$c = 0.2d$	$c = 0.4d$	$c = 0.6d$	$c = 0.8d$	$c = d$
0.01	1.00000	1.00000	1.00000	1.00000	1.00000	0.50564
0.02	1.00000	1.00000	1.00000	1.00000	1.00000	0.51128
0.05	1.00000	1.00000	1.00000	1.00000	0.99818	0.52821
0.10	1.00000	1.00000	1.00000	0.99869	0.94211	0.55642
0.20	1.00000	0.99972	0.99495	0.96286	0.84813	0.61284
0.50	1.00000	0.99780	0.98286	0.94460	0.87679	0.77927
1.00	1.00000	0.99942	0.99541	0.98488	0.96537	0.93529
2.00	1.00000	0.99991	0.99930	0.99765	0.99447	0.98935
5.00	1.00000	0.99999	0.99995	0.99984	0.99962	0.99926
10.00	1.00000	1.00000	0.99999	0.99998	0.99995	0.99991

Table 2
Average distance $\langle|\vec{x} - \vec{y}|\rangle_c/d$ of Eq. (24) for different standard deviations σ and steric repulsion limits c.

σ/d	$c = 0$	$c = 0.2d$	$c = 0.4d$	$c = 0.6d$	$c = 0.8d$	$c = d$
0.01	1.00020	1.00020	1.00020	1.00020	1.00020	1.01136
0.02	1.00080	1.00080	1.00080	1.00080	1.00080	1.02285
0.05	1.00500	1.00500	1.00500	1.00500	1.00541	1.05814
0.10	1.02000	1.02000	1.02000	1.02060	1.03718	1.11937
0.20	1.08000	1.08025	1.08383	1.10242	1.15460	1.24939
0.50	1.47160	1.47451	1.49205	1.53175	1.59549	1.68194
1.00	2.44028	2.44162	2.45016	2.47088	2.50649	2.55797
2.00	4.60697	4.60736	4.60999	4.61678	4.62924	4.64853
5.00	11.32137	11.32143	11.32189	11.32311	11.32544	11.32920
10.00	22.58638	22.58640	22.58652	22.58683	22.58744	22.58843

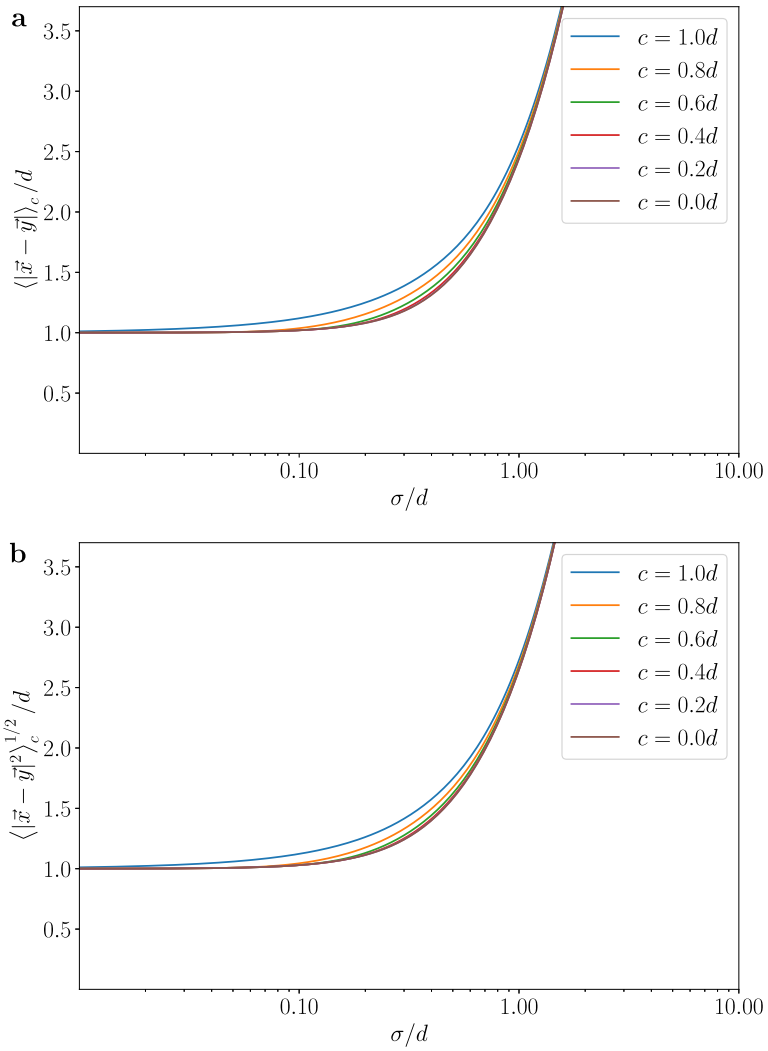

Fig. 2. Plots of (a) the average distance $\langle|\vec{x}-\vec{y}|\rangle_c$ and (b) the root-mean-square distance $\langle|\vec{x}-\vec{y}|^2\rangle_c^{-1/2}$ as a function of the standard deviation σ for different values of the steric repulsion limit c.

Table 3
Root-mean-square distance $\langle|\vec{x}-\vec{y}|^2\rangle_c^{1/2}/d$ of Eq. (25) for different standard deviations σ and steric repulsion limits c.

σ/d	$c = 0$	$c = 0.2d$	$c = 0.4d$	$c = 0.6d$	$c = 0.8d$	$c = d$
0.01	1.00030	1.00030	1.00030	1.00030	1.00030	1.01139
0.02	1.00120	1.00120	1.00120	1.00120	1.00120	1.02300
0.05	1.00747	1.00747	1.00747	1.00747	1.00784	1.05903
0.10	1.02956	1.02956	1.02956	1.03004	1.04465	1.12284
0.20	1.11355	1.11370	1.11613	1.13046	1.17512	1.26235
0.50	1.58114	1.58286	1.59434	1.62301	1.67299	1.74537
1.00	2.64575	2.64652	2.65177	2.66537	2.69027	2.72834
2.00	5.00000	5.00022	5.00175	5.00585	5.01366	5.02621
5.00	12.28821	12.28824	12.28850	12.28919	12.29053	12.29274
10.00	24.51530	24.51531	24.51537	24.51555	24.51589	24.51645

the true distance. This is not a serious problem for conventional NMR structure calculations where it is implicitly taken into account by applying NOE-derived distances only as upper distance bounds. The underestimation for medium standard deviations, on the other hand, can result in inconsistent upper distance bounds and/or structural distortions. Fig. 4 shows that the underestimation is negligible for strong NOEs (e.g., $d = 2.4$ Å), noticeable for medium-strength NOEs (e.g., $d = 3.5$ Å) in the range of $\sigma \approx 0.2$–2 Å, and can be significant for weak NOEs (e.g., $d = 5$ Å) in the range of $\sigma \approx 0.4$–4 Å.

Fig. 4 also shows that the analytical result is in agreement with simulations using Eq. (28). Not surprisingly, the simulations are very accurate for small standard deviations σ and become noisy for large standard deviations (dotted lines in Fig. 4).

4. Discussion

In this paper we have derived, for a harmonic model of atom position fluctuations that is very similar to the one assumed in the theory of the crystallographic B-factor, exact results for the spa-

Table 4
$d^6\langle|\vec{x}-\vec{y}|^{-6}\rangle_c$ of Eq. (26) for different standard deviations σ and steric repulsion limits c.

σ/d	$c = 0.2d$	$c = 0.4d$	$c = 0.6d$	$c = 0.8d$	$c = d$
0.01	1.00301	1.00301	1.00301	1.00301	0.93587
0.02	1.01214	1.01214	1.01214	1.01214	0.87820
0.05	1.08068	1.08068	1.08068	1.07440	0.73578
0.10	1.42281	1.42098	1.37637	1.07182	0.56834
0.20	10.22288	3.64073	1.72165	0.80914	0.37256
0.50	33.39056	3.81099	0.99217	0.35828	0.15435
1.00	8.95396	1.05735	0.28887	0.11049	0.05070
2.00	1.37099	0.16824	0.04846	0.01972	0.00968
5.00	0.09299	0.01158	0.00341	0.00143	0.00073
10.00	0.01172	0.00146	0.00043	0.00018	0.00009

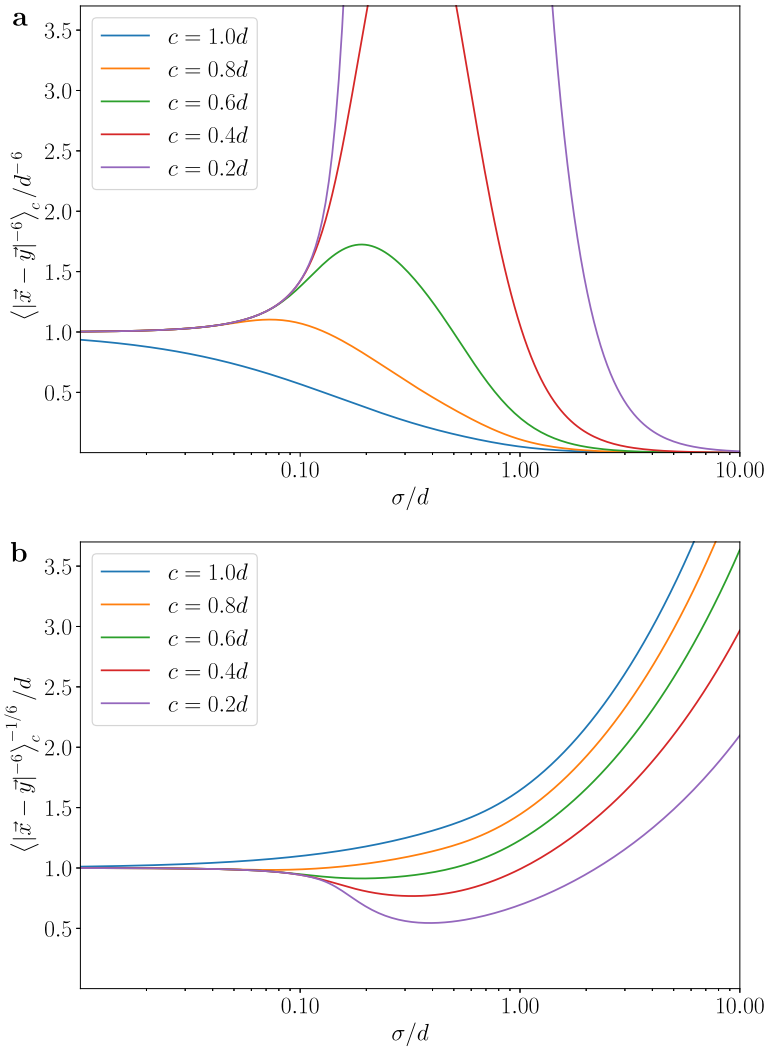

Fig. 3. Plots of (a) the NOE intensity $\langle|\vec{x}-\vec{y}|^{-6}\rangle_c$, relative to an NOE between two non-fluctuating atoms at distance d, and (b) the NOE-derived distance $d_{\text{eff}} = \langle|\vec{x}-\vec{y}|^{-6}\rangle_c^{-1/6}$ as a function of the standard deviation σ for different values of the steric repulsion limit c.

tial impact of the motion on nuclear Overhauser effects and the distances that are derived from them for the purpose of NMR structure determination. Effects are small for strong NOEs that correspond to small distances but can reach to up to 20% underestimation of the true distance for weak NOEs between atoms further apart. The results also explain, on geometrical grounds, the general absence of non-local NOEs in highly flexible structures, such as disordered chain termini or loops and intrinsically disordered or denatured proteins, unless residual local structure is present [21].

This treatment is, despite the exact handling of the spatial averaging, an approximation for the NOE, which is a dynamic cross-relaxation effect that also depends on the time-scales of the motion involved.

The impact of (apart from steric repulsion) isotropic motion on the NOE is under certain conditions not negligible, and one can consider whether it should and how it could be included into NMR structure calculation or refinement. Typical B-factors in crystal structures are well below 100 Å^2 [22], indicating that thermal

Table 5
d_{eff}/d for $d_{\mathrm{eff}} = \langle|\vec{x}-\vec{y}|^{-6}\rangle_c^{-1/6}$ obtained from Eq. (26) for different standard deviations σ and steric repulsion limits c.

σ/d	$c = 0.2d$	$c = 0.4d$	$c = 0.6d$	$c = 0.8d$	$c = d$
0.01	0.99950	0.99950	0.99950	0.99950	1.01111
0.02	0.99799	0.99799	0.99799	0.99799	1.02188
0.05	0.98715	0.98715	0.98715	0.98811	1.05247
0.10	0.94292	0.94312	0.94815	0.98851	1.09875
0.20	0.67879	0.80625	0.91343	1.03593	1.17887
0.50	0.55727	0.80013	1.00131	1.18658	1.36537
1.00	0.69395	0.99075	1.22994	1.44360	1.64376
2.00	0.94877	1.34590	1.65613	1.92388	2.16631
5.00	1.48569	2.10226	2.57704	2.97929	3.33592
10.00	2.09816	2.96767	3.63550	4.19928	4.69686

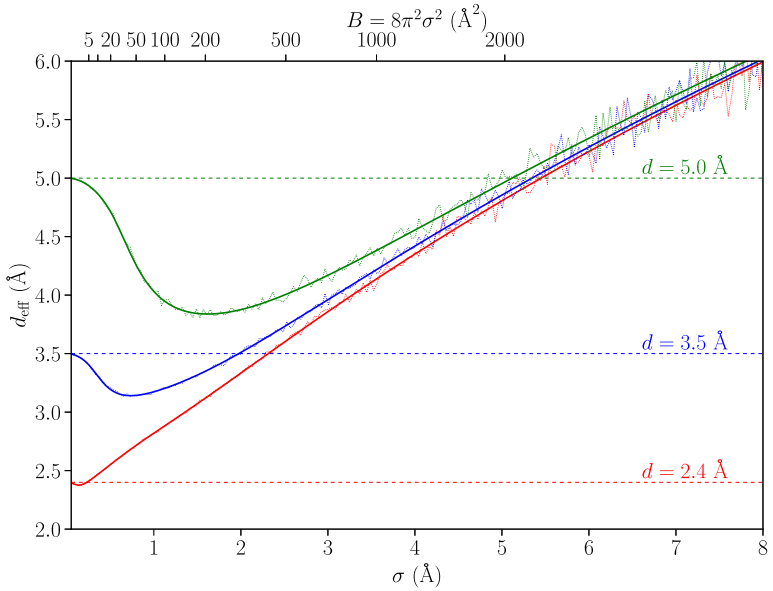

Fig. 4. Plot of the "effective" distance $d_{\mathrm{eff}} = \langle|\vec{x}-\vec{y}|^{-6}\rangle_c^{-1/6}$ (solid lines) as a function of the standard deviation σ for three values of the distance between the two centers of the atom distributions, $d = 2.4$, 3.5, and 5.0 Å (indicated by horizontal dashed lines), that correspond to a strong, medium, and weak NOE, respectively. The steric repulsion limit was set to $c = 2$ Å. The dotted lines show corresponding results of numerical simulations using Eq. (28) with $n = 10^4$ sample point pairs. The horizontal axis at the top shows corresponding values of the crystallographic B-factor, $B = 8\pi^2\sigma^2$.

fluctuations of atom positions in crystals are below 1 Å, especially if one takes into account that only part of the B-factors originates from thermal fluctuations, i.e., that contributions also result from absorbing other errors in fitting diffraction data to models [9]. Observed crystallographic B-factor values correspond to the left-most 10% of the σ-range depicted in Fig. 4. In this respect, it should be kept in mind that internal motion in crystal structures is in general reduced by conducting diffraction measurements at low temperatures [23] and possible restrictions imposed by crystal packing. Larger and more relevant internal motion is expected in solution NMR experiments that are performed near physiological conditions, and in particular for in-cell NMR [24] that studies proteins in a cellular environment more heterogeneous than aqueous solution. While motions of flexible parts of a protein can certainly have amplitudes much larger than 1 Å in solution (while being "frozen" in crystals), this is less likely for ordered core regions, where such large motions would probably weaken the dense but nevertheless delicate network of non-bonded interactions, e.g., hydrogen bonds, that stabilizes the tertiary structure, and thus impair the stability of native protein structures that is observed under physiological conditions.

Would it be possible to determine an "NOE B-factor" by comparing NOEs with a three-dimensional structure? Possibly, if accurately measured NOEs and an equally accurate structure are available. In such an approach, the NOE measurement would yield the experimental value for d_{eff}, while the structure provides the value for d. In the present theory, these two quantities are connected by Eqs. (29) and (26) that can be solved for the standard deviation σ. Whenever $d_{\mathrm{eff}} < d$, there are two possible solutions for σ (or none, if d_{eff} is inconsistently short), as can be seen in Fig. 4. In most cases, the smaller of the two possible σ values would be the relevant one, and the larger solution can be dismissed as corresponding to unrealistically large fluctuations. Nevertheless, the NOE has the potential to characterize fluctuations significantly larger then those observable in high-resolution X-ray structures, where the Gaussian form of the B-factor term implies that the scattering power of an atom with high B-factor (e.g., above 100 Å^2) and its contribution to the calculated structure factors are negligible [22].

However, there are also potential pitfalls in this "NOE B-factor" scenario. On the experimental side, traditional, semi-quantitative NOEs are too imprecise, but eNOEs, which compensate for spin-diffusion and most of the dynamic and technical (pulse sequence-related) influences [18,25,26] and can reach distance accuracies better than 2% [27], can be accurate enough for the purpose. Likewise, accurate mean positions of the atoms (to calculate d) can be obtained from a high-resolution X-ray or high-quality NMR structure. More challenging are probably theoretical limita-

tions inherent in the simple model that was assumed for this study: In practice, fluctuations may often deviate from being isotropic and harmonic. These effects have also been studied extensively in X-ray crystallography, where they can be accounted for, to a certain degree, by anisotropic displacement parameters [9,28]. Fluctuations may also differ in size or being correlated for the two atoms involved in an NOE; both are not accounted for explicitly in the present exact theory, but could be considered numerically. In addition, the present formalism does not explicitly treat NOEs involving methyl protons, degenerate methylene proton pairs, and degenerate aromatic ring protons.

In conclusion, it is clearly advantageous for the study and discussion of the motional influence on the NOE to have at one's disposal the exact, analytical results for a relevant model that we have derived in this paper.

Declaration of Competing Interest

The author declares that he has no known competing financial interests or personal relationships that could have appeared to influence the work reported in this paper.

Acknowledgment

Special thanks to Prof. Kurt Wüthrich for fruitful discussions many years ago, when much of the theoretical part of this work was done while the author was a Ph.D. student in his laboratory.

References

[1] I. Solomon, Relaxation processes in a system of two spins, Phys. Rev. 99 (2) (1955) 559–565, https://doi.org/10.1103/PhysRev.99.559.
[2] J.H. Noggle, R.E. Schirmer, The nuclear Overhauser effect, Academic Press, New York, 1971.
[3] D. Neuhaus, M.P. Williamson, The nuclear Overhauser effect in structural and conformational analysis, VCH, Weinheim, 1989.
[4] S. Macura, R.R. Ernst, Elucidation of cross relaxation in liquids by two-dimensional N.M.R. spectroscopy, Mol. Phys. 41 (1980) 95–117, https://doi.org/10.1080/00268978000102601.
[5] A. Kumar, R.R. Ernst, K. Wüthrich, A two-dimensional nuclear Overhauser enhancement (2D NOE) experiment for the elucidation of complete proton-proton cross-relaxation networks in biological macromolecules, Biochem. Biophys. Res. Commun. 95 (1) (1980) 1–6, https://doi.org/10.1016/0006-291X(80)90695-6.
[6] K. Wüthrich, NMR studies of structure and function of biological macromolecules (Nobel Lecture), J. Biomol. NMR 27 (1) (2003) 13–39, https://doi.org/10.1023/a:1024733922459.
[7] P. Güntert, Structure calculation of biological macromolecules from NMR data, Q. Rev. Biophys. 31 (2) (1998) 145–237, https://doi.org/10.1017/S0033583598003436.
[8] E.T. Olejniczak, C.M. Dobson, M. Karplus, R.M. Levy, Motional averaging of proton nuclear Overhauser effects in proteins - predictions from a molecular dynamics simulation of lysozyme, J. Am. Chem. Soc. 106 (7) (1984) 1923–1930, https://doi.org/10.1021/ja00319a004.
[9] K.N. Trueblood, H.B. Bürgi, H. Burzlaff, J.D. Dunitz, C.M. Gramaccioli, H.H. Schulz, U. Shmueli, S.C. Abrahams, Atomic displacement parameter nomenclature - Report of a subcommittee on atomic displacement parameter nomenclature, Acta Crystallographica Section A 52 (1996) 770–781, https://doi.org/10.1107/s0108767396005697.
[10] P. Debye, Interferenz von Röntgenstrahlen und Wärmebewegung, Ann. Phys. 43 (1) (1913) 49–92, https://doi.org/10.1002/andp.19133480105.
[11] I. Waller, Zur Frage der Einwirkung der Wärmebewegung auf die Interferenz von Röntgenstrahlen, Zeitschrift für Physik 17 (1923) 398–408, https://doi.org/10.1007/bf01328696.
[12] Z.T. Sun, Q. Liu, G. Qu, Y. Feng, M.T. Reetz, Utility of B-factors in protein science: Interpreting rigidity, flexibility, and internal motion and engineering thermostability, Chem. Rev. 119 (3) (2019) 1626–1665, https://doi.org/10.1021/acs.chemrev.8b00290.
[13] C.B. Post, Internal motional averaging and 3-dimensional structure determination by nuclear magnetic resonance, J. Mol. Biol. 224 (4) (1992) 1087–1101, https://doi.org/10.1016/0022-2836(92)90471-u.
[14] C. Reinknecht, A. Riga, J. Rivera, D.A. Snyder, Patterns in protein flexibility: A comparison of NMR "ensembles, MD trajectories, and crystallographic B-factors, Molecules 26 (5) (2021) 11, https://doi.org/10.3390/molecules26051484.
[15] M. Nilges, A calculation strategy for the structure determination of symmetrical dimers by ^{1}H-NMR, Proteins: Structure, Function, and Genetics 17 (3) (1993) 297–309, https://doi.org/10.1002/prot.340170307.
[16] M. Nilges, Calculation of protein structures with ambiguous distance restraints - Automated assignment of ambiguous NOE crosspeaks and disulfide connectivities, J. Mol. Biol. 245 (5) (1995) 645–660, https://doi.org/10.1006/jmbi.1994.0053.
[17] P. Güntert, L. Buchner, Combined automated NOE assignment and structure calculation with CYANA, J. Biomol. NMR 62 (4) (2015) 453–471, https://doi.org/10.1007/s10858-015-9924-9.
[18] B. Vögeli, S. Kazemi, P. Güntert, R. Riek, Spatial elucidation of motion in proteins by ensemble-based structure calculation using exact NOEs, Nature Structural & Molecular Biology 19 (10) (2012) 1053–1057, https://doi.org/10.1038/nsmb.2355.
[19] L. Ahlfors, Complex analysis, McGraw-Hill, New York, 1979.
[20] D. Leitz, B. Vögeli, J. Greenwald, R. Riek Temperature dependence of $^{1}H_{N}$-$^{1}H_{N}$ distances in ubiquitin as studied by exact measurements of NOEs, Journal of Physical Chemistry B 115 (23) (2011) 7648–7660. doi:10.1021/jp201452g.
[21] D. Neri, M. Billeter, G. Wider, K. Wüthrich, NMR determination of residual structure in a urea-denatured protein, the 434-repressor, Science 257 (5076) (1992) 1559–1563, https://doi.org/10.1126/science.1523410.
[22] O. Carugo, How large B-factors can be in protein crystal structures, BMC Bioinformatics 19 (2018) 9, https://doi.org/10.1186/s12859-018-2083-8.
[23] J.S. Fraser, H. van den Bedem, A.J. Samuelson, P.T. Lang, J.M. Holton, N. Echols, T. Alber Accessing protein conformational ensembles using room-temperature X-ray crystallography, Proceedings of the National Academy of Sciences of the United States of America 108 (39) (2011) 16247–16252. doi:10.1073/pnas.1111325108.
[24] D. Sakakibara, A. Sasaki, T. Ikeya, J. Hamatsu, T. Hanashima, M. Mishima, M. Yoshimasu, N. Hayashi, T. Mikawa, M. Wälchli, B.O. Smith, M. Shirakawa, P. Güntert, Y. Ito, Protein structure determination in living cells by in-cell NMR spectroscopy, Nature 458 (7234) (2009) 102–105, https://doi.org/10.1038/nature07814.
[25] B. Vögeli, The nuclear Overhauser effect from a quantitative perspective, Prog. Nucl. Magn. Reson. Spectrosc. 78 (2014) 1–46, https://doi.org/10.1016/j.pnmrs.2013.11.001.
[26] B. Vögeli, P. Güntert, R. Riek, Multiple-state ensemble structure determination from eNOE spectroscopy, Mol. Phys. 111 (3) (2013) 437–454, https://doi.org/10.1080/00268976.2012.728257.
[27] B. Vögeli, M. Friedmann, D. Leitz, A. Sobol, R. Riek, Quantitative determination of noe rates in perdeuterated and protonated proteins: Practical and theoretical aspects, J. Magn. Reson. 204 (2) (2010) 290–302, https://doi.org/10.1016/j.jmr.2010.03.009.
[28] A.E. Garcia, J.A. Krumhansl, H. Frauenfelder, Variations on a theme by Debye and Waller: From simple crystals to proteins, Prot.-Struct. Funct. Genet. 29 (2) (1997) 153–160, https://doi.org/10.1002/(sici)1097-0134(199710)29:2<153::aid-prot3>3.0.co;2-e.